Cold Target Recoil Ion Momentum Spectroscopy

H. Schmidt-Böcking[1], M. Achler[1], I. Ali[1], H. Bräuning[1],
C. L. Cocke[3], R. Dörner[1], O. Jagutzki[1], T. Kambara[5],
Kh. Khayyat[1], V. Mergel[1], R. Moshammer[1], M. H. Prior[4],
L. Spielberger[1], W. Schmitt[2], K. Ullmann-Pfleger[1],
M. Unverzagt[1], J. Ullrich[2], W. Wu[3],
[1]Universität Frankfurt, Institut für Kernphysik,
August-Euler-Str.6, 60486 Frankfurt, FRG
[2]GSI-Darmstadt, 64220 Darmstadt, FRG
[3]Kansas State University, Manhattan/Ks, 66506, USA
[4]Lawrence Berkeley National Laboratory, Berkeley/Ca, 94720, USA
[5]RIKEN, Wako, Saitama, Japan

Abstract

A newly developed spectroscopy technique is presented to study the kinematics of many-particle atomic collision processes with high momentum resolution and high detection efficiency. These goals are achieved by detecting the low energetic recoil ion in coincidence with the emitted electrons or scattered projectiles. The recoil ions can be detected with nearly 100% efficiency by projecting them with a weak electrostatic field on a position-sensitive detector. The high momentum resolution for the recoil ion is obtained by using a cold super- sonic target jet and calculating the recoil-ion trajectory from the measured time-of-flight and position on the position-sensitive detection devices. The basic components of the experimental set-up for **COLTRIMS** (**COL**d **T**arget **R**ecoil **I**on **M**omentum **S**pectroscopy) and first results obtained with this technique are presented. Results for electron capture, target and projectile ionization in fast ion-atom collisions as well as photo ionization processes are described. Future applications of **COLTRIMS**, e.g. in the field of atomic physics for the investigation of inneratomic many electron dynamics or in the field of nuclear physics to study the kinetics of the nuclear beta-decay, are discussed.

1 Introduction

High-resolution spectroscopy techniques in atomic collision physics in general suffer from the restriction of small detection efficiency. Thus, the coincident detection of several reaction products to study e.g. many-particle effects becomes extremely difficult. This is one of the reasons for the lack of systematic experimental data on the many-particle momentum exchange in atomic collision processes. Only very few data have been published so far in the literature for double target ionization [1, 2, 3, 4] e.g. for (e,3e) and (γ,2e) reactions. Systematic data exist for single ionization processes, e. g. (e,2e) reactions (see e.g. [5]). In these experiments the traditional electron-electron-coincidence technique was used to measure the electron-electron momentum correlation in the final state. In case of three electrons in the continuum final state, triple e-e-e coincidence techniques yield extremely low coincidence detection efficiency, particularly if high momentum resolution is required. To our knowledge only one experiment has been reported in literature [4].

In case of detecting the recoil ion instead of electrons, however, this ion can be detected with high resolution and a solid angle of nearly 100% and a total detection efficiency of about 60%. To achieve high momentum resolution the initial target motion (initial target temperature) has to be strongly reduced and the recoil-ion trajectory and its time-of-flight (TOF) must be measured precisely. Using standard super-sonic target devices, for helium as target gas an initial target temperature of a few mK can be obtained which is equivalent to a momentum distribution width of approximately $0.01 a.u.$, i.e. about $40 eV/c$. Depending on the size and the geometry of the recoil-ion spectrometer a relative resolution below 1% can be achieved for the recoil-ion momentum. Thus, for small recoil-ion momenta a resolution of $0.02 a.u.$ is feasible with a relatively small detection device. In not too far future Laser-cooled gas targets may even provide lower target temperatures and by using large scale detection devices a relative momentum resolution of a few 10^{-4} is achievable. The ultimate limit of momentum resolution obtainable with presently thinkable techniques may approach $0.001 a.u.$, which corresponds to $4 eV/c$.

Since the kinetic energy of practically all created recoil ions after the collision is mostly below $1 eV$ they all can be projected even by a weak electrostatic field onto a position-sensitive detection device. Thus, the recoil-ion

momentum spectroscopy provides a much more efficient alternative technique for momentum spectroscopy in atomic many- particle collision processes than traditional electron spectroscopy. Particularly if two or more reaction partners in the final state have to be measured in coincidence it is usually sufficient to measure the recoil-ion momentum vector and only two momentum components e.g.the emission angle (i.e. the detection position) of the other ejected partners, to yield already complete information on the momentum exchange in such three-particle collisions.

For fast ion-atom collision processes, as will be shown below, the recoil-ion transverse (with respect to the incoming beam) momentum component is a good measure for the impact parameter, and its longitudinal component reflects the Q-value (inelasticity due to electronic excitation and ionization) and the mass exchange (number of transferred electrons) in such collisions. Thus, the measurement of the longitudinal momentum is equivalent to an energy-gain spectroscopy and it can provide for the projectile energy gain or loss in fast ion atom collisions a relative resolution even in the 10^{-9} regime. Therefore recoil-ion momentum spectroscopy is a tool which yields even in GeV ion-atom collisions precise information on the electronic transitions. Furthermore, also for (e,2e) or (e,3e) or (γ,2e) measurements **COLTRIMS** provides a very efficient way to study the complete momentum exchange between the electrons and nuclei in such collision processes. For a recoil-ion-electron coincidence an overall coincidence efficiency of 10 to 20% is easily feasible, therefore coincidence rates can nearly approach singles rates. Furthermore, **COLTRIMS** is not limited to any spatial direction therefore complete angular distributions are obtained.

In section 2 a short outline of the important kinematical equations for the recoil-ion spectroscopy is given and in section 3 the experimental technique is presented. In section 4 of this paper first results [6, 7, 8, 9, 10, 11, 12] for different collision processes are discussed and the power of the new technique is described.

2 Recoil Ion Kinematics

Since in all atomic collision processes energy and momentum are conserved, we can derive some general equations for the final momentum and energy state of the recoil ions. In the next two subsections we will discuss the

equations for ion-atom collisions and photo absorption. Atomic units are used throughout ($e = \hbar = m_e = 1$).

2.1 Ion-Atom Collisions

The kinematical calculations for the recoil ion in fast ion-atom collisions become most simple if the momentum transfer between the collision partners is small compared to the initial momentum in the center-of-mass system. In this case the longitudinal momentum of the recoil ion depends only on the inelastic energy gain or loss of the collision process (i.e. electronic excitation, emission of Bremsstrahlung etc.), on the mass transfer in electron capture collisions, and on the longitudinal momenta of the electrons emitted to the continuum. The transverse momentum of the recoil ion in "close" encounters reflects the nuclear impact parameter. The condition of small momentum transfer is fulfilled in most of all atomic reactions of interest here. The three most important possibilities for target ionizing collisions are:

- capture from n_C target electrons to projectile bound states,
- ionization of m_T target electrons,
- ionization of l_P projectile electrons.

From energy- and momentum-conservation we obtain for the longitudinal momentum of the recoil ion in the final state ($p^f_{\parallel R}$):

$$p_{\parallel R}{}^f = \underbrace{\frac{Q}{v_P}}_{\text{Q-value}} \underbrace{- n_C \frac{v_P}{2}}_{\text{mass transfer}} + \underbrace{\sum_{j=1}^{m_T} \left(\frac{E^f_{ej}}{v_P} - p^f_{\parallel ej} \right)^{\Sigma_{Lab}}}_{\text{target ionization}} + \underbrace{\sum_{j=1}^{l_P} \left(\frac{E^f_{ej}}{v_P} \right)^{\Sigma_P}}_{\text{projectile ionization}} . \tag{1}$$

Q: Q-value (i.e. the sum of all electronic de- and excitation energies, v_P: projectile velocity, E^f_{ej}: final continuum energy of the jth electron, $p^f_{\parallel ej}$: final momentum of the jth electron, (given in the lab frame for electrons from the target and in the projectile frame for electrons emitted from the projectile).
This equation can be simplified if we focus now on several special reaction channels.

For pure electron capture only discrete values of $p^f_{\parallel R}$ occur corresponding to the energy eigenvalues of the projectile and target electrons.

$$p^f_{\parallel R} = \frac{Q}{v_P} - n_C \frac{v_P}{2}. \tag{2}$$

This enables us to determine the energy levels of all excited states with high precision, often better than standard energy gain spectroscopy techniques can do.

For the emission of target electrons to continuum states we obtain:

$$p^f_{\parallel R} = \frac{Q}{v_P} + \sum_{j=1}^{m_T} \left(\frac{E^f_{ej}}{v_P} - p^f_{\parallel ej} \right)^{\Sigma_{Lab}} = -\frac{\Delta E_P}{v_P} - \sum_{j=1}^{m_T} p^{f\,\Sigma_{Lab}}_{\parallel ej}, \tag{3}$$

where ΔE_P is the kinetc energy change of the projectile. If $(Q + \sum_{j=1}^{m_T} E_{ej})/(v_P p^f_{\parallel R}) \ll 1$ is valid, i.e. the projectile velocity is much higher than the one of the outgoing electrons, the longitudinal momentum of the recoil ion reflects the sum of the longitudinal electron momenta. We obtain:

$$p^f_{\parallel R} \approx -\sum_{j=1}^{m_T} p^f_{\parallel ej}. \tag{4}$$

For the ionization of n_P electrons of the projectile it follows from equation 1:

$$p^f_{\parallel R} = \frac{Q}{v_P} + \sum_{j=1}^{l_P} \left(\frac{E^f_{ej}}{v_P} \right)^{\Sigma_P}. \tag{5}$$

For this case one can calculate the total energy loss/gain of the projectile directly from the measured $p_{\parallel R}$.

For all collisions the transverse momentum of the recoil ion reflects the sum of transverse momenta of projectile and electrons:

$$p^f_{\perp R} = -\sum_{j=1}^{l_P = m_T} p_{\perp ej} - p_{\perp P}. \tag{6}$$

In figure 1 the raw spectrum of on component of $p^f_{\perp R}$ and $p^f_{\parallel R}$ is shown for 15 keV protons on He showing capture and ionization, respectively. For

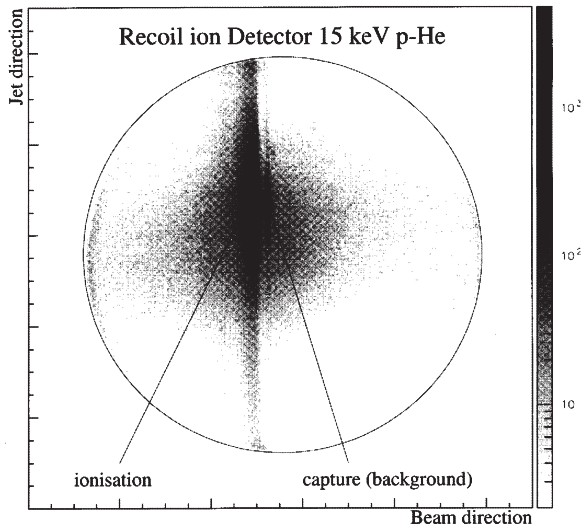

Figure 1: Image of He^{1+} ion on the recoil ion detector for $15keV$ p→He, measured in coincidence with an emitted electron. (see text)

electron capture the longitudinal recoil-ion momentum components (beam direction) are constant for all measured recoil-ion transverse momenta. For target ionization the recoil-ion longitudinal momenta as function of the longitudinal momentum of the emitted electron are presented in figure 2. They show the predicted dependence E (see equation 3). In figure 3 the projections of the recoil-ion longitudinal momenta are displayed. The energy-gain resolution of about 10^{-4} allows to separate the different reaction channels. Even the weak target ionization channel with simultanous excitation of the second He electron to the L shell is observable.

2.2 Photo Absorption

In the case of absorption of a single photon the approximation of small momentum is still fullfilled. But the electron can absorb all the photon energy E_γ leading to the momentum $p_e = \sqrt{2(E_\gamma - E_{Bind} - E_{excitation})}$. E_{Bind} is the binding energy of the emitted electron and $E_{excitation}$ the excitation en-

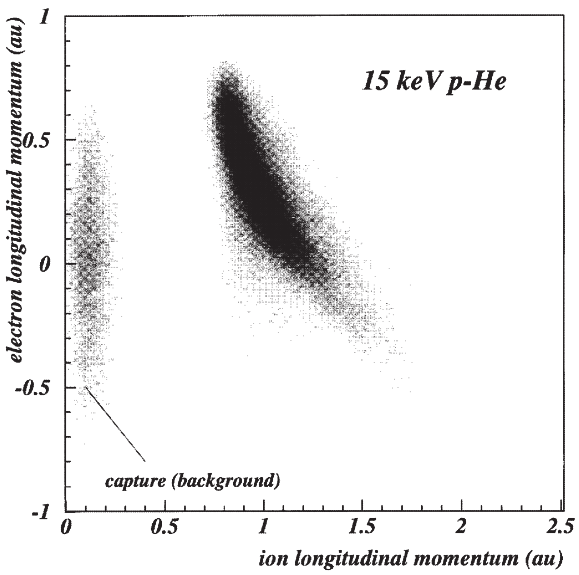

Figure 2: Correspondence of electron longitudinal momentum and He^{1+} longitudinal momentum for $15keV$ p + He $\rightarrow$ He^{1+} + e^-. The distribution has been integrated over the transverse momenta of all particles. Since in this reaction the electron transverse momenta are small, one can see a structure as expected from equ. 2

ergy of the residual ion. The recoil ion has to compensate this momentum. So the ions are distributed on a momentum sphere of a radius $p_R = p_e$ in the center-of-mass system, where E_γ is the photon energy. Because of the momentum of the incoming photon (p_γ) this sphere is shifted in the Lab system by $p_\gamma = E_\gamma/c$.

In figure 4 the measured recoil-ion momenta in the x-y-plane are plotted. x and y are the directions of the electric field vector and of the momentum of the linear polarized incoming photon, respectively. One can see two kinematic circles: the one with the larger radius corresponds to the emission of one K-electron, where the other electron remains in the He^{1+} ground state; the one with the smaller radius corresponds to ionization of one K-electron and simultaneous excitation of the second He electron to the L-shell.

These two cases presented are only a few examples for the variety of

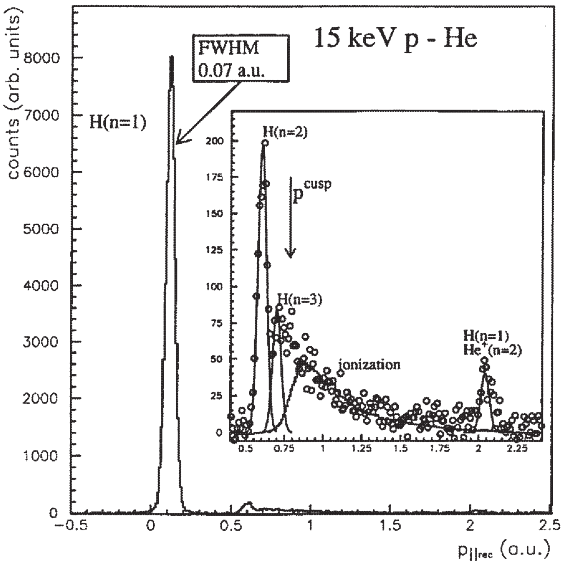

Figure 3: Longitutinal momentum distribution of He^{1+} iions from $15keV$ proton impact. The dominant peak is due to capture to the projectile ground state. The arrow indicates the position of the capture to theprojectile continuum. The full line right of the arrow shows the momentum distribution for ionization only, which has been measured separately by detecting an electron in coincidence with the recoil ion. The momentum resolution is $\pm 0.035 a.u.$, equivalent to an energy gain of $\pm 0.7eV$ and a recoil energy of $\pm 4.5 \mu eV$ [12]

information one can extract from the momentum of the recoil ion in atomic collision processes.

3 Experimental Set-up

3.1 Principle of COLTRIMS

The measurement of momentum transfer between different atomic reaction products is always performed by determining the final and the initial momenta of these products. Furthermore the accuracy of the determination of

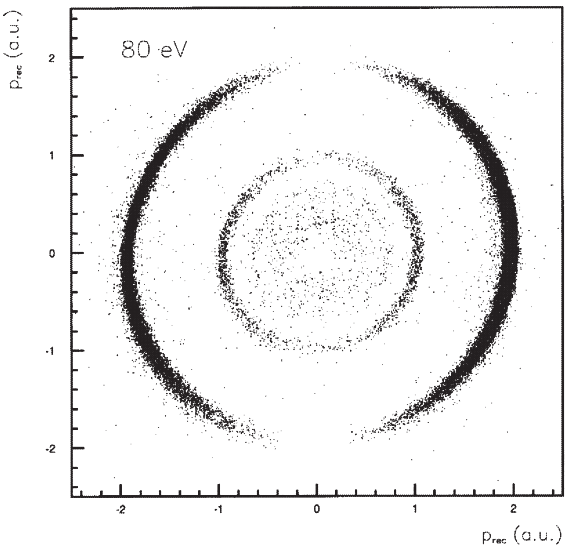

Figure 4: Momentum distribution of He^{1+} ion produced by $80eV$ photon impact. The x axis is the direction of the polarization vector of the linear polarized light, the y axis is the direction of the photon beam. The distribution has been integrated over a momentum range of $\pm 0.3 a.u.$ in the z direction. For more detail see [10].

the momentum transfer is generally better, when the transferred momentum is of the order of the final and large compared to the initial momentum. The measurement of the initial momenta, however, becomes even obsolete when they are very small compared to the transferred momentum. These requirements are perfectly fullfilled in the COLTRIMS spectroscopy technique.

The main components of **COLTRIMS** are the very cold target gas jet and the recoil-ion spectrometer with a position-sensitive detector. In the center of the recoil-ion spectrometer the incoming projectiles collide with the cold target atoms.

3.2 Super-sonic Gas Jet

In the **COLTRIMS**- systems presently used (see Figure 5) a supersonic helium gas jet, with an internal temperature of lower than $0.1K$, provides the rather cold localized gas target. The helium gas expands through a $30\mu m$ hole. The gas nozzle is mounted on the cold finger of a cryo pump and is cooled down to a temperature of 10 to $35K$. The gas jet is collimated at a distance of about $10mm$ from the expansion hole by a skimmer of approximately $0.3mm$ diameter. The gas jet leaves the collision chamber through a hole of about 1cm diameter into a jet dump, pumped by a small turbomolecular pump (260 or $360l/sec$) to reduce the helium residual gas pressure in the scattering chamber to a few $10^{-8}mbar$. Typical pressures are: $400mbar$ on the high pressure side of the $30\mu m$ hole and $5 \times 10^{-4}mbar$ in the source chamber (preskimmer stage). The source and the scattering chambers are separately pumped by two small (260 or $360l/sec$) turbomolecular pumps. At the collision region, $30mm$ above the skimmer, the helium gas jet has a diameter of 1 to $2mm$ and a local density of 1 to $5 \times 10^{11} atoms/\mathrm{cm}^2$. The internal temperature is lower than $0.1K$ in the jet direction [13]. Perpendicular to the jet the atoms have a momentum spread of $\pm 0.02 a.u.$ given by the velocity of the jet and the skimming geometry. Figure 5 shows the gas jet device with the target and source chamber.

3.3 Recoil-Ion Spectrometer

The recoil ions created at the intersection point of the gas jet with the ion beam are extracted by a weak homogeneous electrostatic field varying between 0.1 to about $10V/cm$ depending on the expected recoil-ion momenta. After passing a field-free drift region they are post accelerated onto a position-sensitive channel-plate detector with a position resolution of $< 0.2mm$. Great care has been taken to assure proper field conditions in the spectrometer area. The time-of-flight of the recoil ions is measured by a coincidence with projectiles, electrons or the machine pulse, when using a pulsed beam. From the time-of-flight and the position on the channel-plate detector the three momentum components of the recoil ion can be calculated.

Different recoil-ion spectrometers have been developed in the last two years. For some applications the extraction of the recoil ions perpendicular to the projectile direction yields optimal detection and resolution for the investigated collision system, in other cases the recoil-ion extraction par-

allel to the projectile beam direction has substantial advantages. In the **COLTRIMS** spectrometer of [9] the recoil ions are extracted from the interaction region perpendicular to the beam. In these spectrometers (see figure 6) the drift region was separated from the extraction region by a woven mesh of $0.25mm$ mesh width. A stack of three of these meshes with 1mm spacing shields the drift region from the strong postaccelaration field just in front of the detector. On all parts, including the meshes, a thin layer of carbon is evaporated to avoid contact potentials. However, recent tests with improved spectrometers [12, 10, 14] have shown, that all meshes influence somewhat the recoil-ion trajectory and are thus limiting the resolution to about $0.05a.u.$. In these recoil-ion spectrometers a homogeneous field in the extraction region is obtained by shielding this area from external potentials e.g. with a carbon fiber. One thin carbon fiber of $7\mu m$ diameter and $10m$ length (or in some cases a thin metallic wire, see e.g. [15] is wound around four supporting germanium coated insulator screws. The fiber defines the potential in the extraction region and divides the voltage. Figure 6 shows a schematic of the recoil-ion spectrometer used by [10, 14] A sudden potential change in the extraction region provides a field geometry, which focuses recoil ions with the same momentum but created at different target positions onto the same position on the detector.

The resolution e.g. of the apparatus used in reference [**?**, **?**, 14] for $p_{\|R}$ is $\pm 0.035a.u.$. This resolution is limited by the precooling target temperature of about $30K$. The momentum resolution in the direction of the extraction field is $\pm 0.02a.u.$, mainly restricted by the internal momentum spread of the jet perpendicular to the jet direction.

In the **COLTRIMS** spectrometer used by Moshammer and coworkers [8, 16, 17] a uniform electric field along the ion beam is generated by two parallel ceramic plates covered with burnt-in resistive layers. This spectrometer is shown in Figure 7. Recoil ions and electrons are accelerated into the forward and backward directions, respectively. The electric field is superimposed by a magnetic solenoid field which forces electrons on spiral trajectories thus yielding nearly 100% detection efficiency for electrons with transverse kinetic energies below $30eV$. In contrast to the spectrometers described above the recoiling ions are extracted in the longitudinal direction parallel to the ion beam. Thus very large longitudinal recoil-ion momenta (up to $160a.u.$) can be detected and the momentum resolution can strongly be improved. In [8] already a recoil-ion momentum resolution of $0.16a.u.$

(FWHM) was obtained. The theoretical limits for the momentum resolution of the recoil ion for the present super-sonic gas target are $< 0.02 a.u.$ in transverse and $0.0005 a.u.$ in longitudinal direction. Due to a specially designed burnt-in resitive layer structure in the spectrometer plates the electric field in the beam-target intersection region can be directed with in any direction. Thus the recoil-ion position on the channelplate can be chosen according to the requirements of the measurement. This spectrometer is perfectly suited for experiments carried out in ion beam storage rings. The system is described in detail [17]

An important component of the **COLTRIMS** system are the position-sensitive recoil-ion or electron detectors. The standard size detector is a $50mm$ diameter chevron or Z-stack channelplate electron multiplier with an active area of typically $47mm$ diameter. The position information is obtained either from charge division using "wedge-and-strip" anode structures or from time measurements using "delay-line" anode structures. Both position readout systems can yield a position resolution better than $0.1mm$ depending on the electronic moduls (preamplifiers, constant fractions, analog digital or time digital converters etc.) available. It might be worth to notice that the use of a Z-stack channelplate system yields, even for electron detection, signals far separated from noise pulses providing even with "standard electronic moduls" very good position resolution. In Figure 8 the "Delay-Line" detector and a typical position spectrum (figure 9) for electron detection are shown.

3.4 Coincidence Experiments using COLTRIMS

In the recoil-ion spectrometers of reference [18] opposite to the detector for the recoil ions a second position-sensitive detector for electrons is located. For the same given momentum the electrons are much faster than the recoil ions due to the lighter mass. Thus, they are nearly unaffected by the weak electrostatic extraction field. The solid angle for electron detection is determined for the high energetic electrons by the geometry of this device and can reach for the present spectrometer about 15%, for low energetic electrons (less than about $5eV$ kinetic energy) the solid angle approaches nearly 100%.

To improve the electron detection efficiency for high energetic electrons Moshammer and coworkers [8] have added to the electrostatic extraction

field a weak magnetic solenoid field (see figure 7). The electrons are bent onto spiral-like trajectories by a magnetic field thus even for $100eV$ electrons a 4π solid angle can be obtained.

As discussed in detail in [17] for all electrons independent of their kinetic energy their Lamour frequency is constant, thus the electron detection position can be corrected for the deflection of the electron motion in the magnetic field. Using this spetrometer [8, 16] have carried out several benchmark recoil-ion -electron coincidence experiments to investigate the dynamics of target ionization by fast highly charged ion impact.

4 Experimental Results and Discussion

In this chapter the following ionization processes investigated by **COLTRIMS** will be discussed:

1. $He^{2+} + He \rightarrow He^{1+} + He^{1+}$
(electron capture)
2. $Ni^{24+} + He \rightarrow Ni^{24+} + He^{1+} + e$
(target ionization)
3. $He^{1+} + He \rightarrow He^{2+} + He^{1+} + 2e$
(projectile ionization)
4. $F^{8+} + He \rightarrow F^{9+} + He^{1+} + 2e$
(projectile ionization)
5. $\gamma + He \rightarrow \gamma' + He^{2+} + 2e$
(photo ionization)

The first reaction was measured at different projectile velocities of a few $a.u.$, and represents a single-electron transfer process, with two reaction partners in the final state [9, 19]. The high resolution of **COLTRIMS** allows for the first time in such fast encounters the separation of electron capture into different excited states. In reaction 2 the single ionization of helium by $200MeVNi^{24+}$ impact has been investigated by a recoil-electron-projectile triple coincidence [8]. The energy loss distribution of the projectile and the corresponding low-energy electron emission has been measured for the pure ionization channel. In reaction 3 and 4 [6, 7] the projectile and the target are simultaneously ionized either by nucleus-electron or by electron-electron interaction. Both interaction processes yield differ-

ent recoil-ion momentum distributions and can, indeed, be experimentally separated by **COLTRIMS**. In reaction 5 He-double ionization has been investigated for high-energy photon Compton scattering [11]. Measuring the recoil-momentum, the Compton scattering and photo-effect processes were separated.

4.1 Energy-Gain Spectroscopy

Reaction 1: In this single-electron transfer reaction only two particles are in the final state. Since the electron transfer can lead to an excited state there are 6 unknown momentum components plus one Q-value parameter in the final state. Because of energy and momentum conservation the measurement of the three recoil momentum components yields the complete determination of the full kinematics in this collision and thus provides fully differential cross sections for electron capture into different excited states. In Figure 10 for $0.25MeV He^{2+} + He$ the recoil-ion longitudinal momentum distribution is shown. Two separated peak structures can be seen. The peak at $p^f_{\parallel\ R} = -1.5a.u.$ results from electron transfer between the 1s-state; the peak at $-0.5a.u.$ shows the capture contributions, when one electron is excited into the L shell. As explained above in Chapter 2, for electron capture the recoil ion receives a backward momentum transfer from the electron mass transfer between target and projectile. A positive Q-value (energy loss) gives the recoil ion a momentum transfer of Q/v_P in forward direction. There is even a small contribution to be seen from forward directed recoil-ion emission, indicating a large positive Q value, i.e. simultaneous excitation of target and projectile. The recoil momentum resolution in the longitudinal direction obtained here is $0.26a.u.$, which yields for this collision system an energy-gain resolution of about $\Delta E/E = 1 \times 10^{-5}$.

In Figure 11 the differential capture cross sections as function of the transverse recoil-ion momentum $p_{\perp rec}$ are presented. The transverse momentum can be easily transformed into projectile scattering angle by dividing it by the incoming projectile momentum p_0. For $1MeV$ projectile energy the recoil transverse momentum of $1a.u.$ corresponds to a scattering angle of $4 \times 10^{-5} rad$. It can be seen that with increasing projectile energy the contribution of capture into the ground state increases. However, below $1MeV$ projectile energy capture into exited states dominates. For $0.25MeV$ bombarding energy, a dip in the differential cross section for ground-state

capture can be seen at a transverse momentum of about $1.5 a.u.$ This structure is due to the interference of the relevant capture amplitudes on the in- and outgoing trajectories. A more detailed discussion of these data is given in [9, 19]. Very recently Kambara and cooworkers [15] have used the **COLTRIMS** technique to investigate the capture process in fas O^{7+}-He collisions.

4.2 Target Ionization in Fast Ion-Atom Collisions

Reaction 2: Using **COLTRIMS** [8] have recently investigated the low energy electron ejection in $200 MeV\ Ni^{24+} + He \rightarrow Ni^{24+} + He^{1+} + e^-$ collisions, performing a recoil-electron-projectile coincidence. The apparatus they used is shown in Figure 7. Applying a weak magnetic solenoid field they obtained for electron energies below $50 eV$ a nearly 30% triple coincidence detection efficiency and could measure for each event the complete momentum balance in these three-particle reactions. They could show that in these encounters the recoil ion and the ejected electron are strongly correlated in their longitudinal and transverse momenta (see figure 12). The projectile undergoes only a very momentum change. The projectile energy-loss distribution is shown in Figure 13 as function of the correlated electron and recoil longitudinal momentum. The measured correlated- momentum width reflects mainly the experimental resolution of $0.16 a.u.$. This width corresponds to an projectile energy loss width of about $70 eV$. The mean projectile energy loss is found to be about $30 eV$ which corresponds to an energy gain/loss resolution of about 1×10^{-7}. The combined technique of weak electrostatic and magnetic fields provides important efficiency improvements for the **COLTRIMS** technique and is particularly suited for the investigation of ionization and capture processes in ion-beam storage rings. Details of this technique are described by [17].

Using **RIMS** Unverzagt and cooworkers [16] and Jardin and coworkers [27] have recently investigated also the multiple target ionization and have found strongly correlated electron emission into the forward direction.

4.3 e-e Interactions in Ion-Atom Collisions

Reaction 3 and 4: It is generally assumed that in fast ion-atom ionization processes the target ionization is due to a target-electron projectile-nucleus interaction. However, if the projectile is not fully stripped its remaining electrons can also contribute to the target ionization process via a pure electron-electron interaction [20, 21, 6, 7] In recent times the importance of these e-e contributions were discussed by comparing total ionization cross sections with theory [20, 21]. So far it has been rather difficult to separate these different ionization mechanisms by traditional experimental detection techniques. **COLTRIMS** , however, provides a new experimental tool, to separate the different mechanisms by the very small differences in their final momentum states. In the case of a nucleus-electron interaction the projectile nucleus has to penetrate the target atom in a "close" collision yielding a transverse momentum exchange between the projectile and the target nuclei of more than $1 a.u.$. In case of e-e interaction only the two electrons in the projectile and target have to approach each other and the nuclei are mostly distant spectators. Thus, in these collisions a smaller transverse momentum is given to the recoiling target ion. Also the longitudinal momentum of the recoil ion in the case of e-e interaction should be smaller than for the nucleus-electron ionization process. In Figure 14 for He^{1+} on He collisions the measured transverse and longitudinal recoil-ion momentum distributions are shown for different bombarding energies. For experimental reasons the reaction channel with simultaneous target and projectile ionization was separated by a recoil-ion-projectile coincidence, since in this channel the e-e contribution is easily visible. Figure 14 shows that the distributions has two separate peak positions whose relative strengths vary with projectile energy. The peak near zero-recoil-momentum is indeed resulting from e-e interactions, whereas the peak at larger recoil momentum is due to nucleus-electron ionization processes. Both contributions show the expected projectile energy (E_p) dependence. The n-e interaction decreases with E_p^{-2}, whereas the e-e decreases with E_p^{-1} towards higher projectile energies. The e-e contribution is only observable above the expected threshold velocity. In Figure 14f the recoil-ion momentum distribution for $130eV$ electron impact on helium is also shown. This distribution agrees nicely with the e-e contribution at $1MeV$ Helium impact energy (i.e. the same projectile velocity). Using the same recoil detection technique Wu and coworkers [7] could recently separate for F^{8+} on helium the e-e and n-e contributions as well and determine the absolute cross sections for both ionization mechanisms.

4.4 Photo Ionization

Reaction 5: **COLTRIMS** is a powerful technique for "complete" experiments of photon induced ionization processes. For example, $(\gamma\, 2e)$ reactions can very efficiently be investigated by recoil-ion-electron coincidence detection systems replacing the traditional low efficiency electron-electron coincidence technique. Since the absolute value of the recoil-ion momentum vector can be detected with nearly 100% efficiency and high resolution, only the emission angle of one electron has to be measured using large solid angle position-sensitive electron detectors. Thus a nearly 20% total coincidence efficiency is obtained. Vogt and coworkers (at Hasylab-Hamburg) [22] and Dörner and coworkers [18] (at the Advanced Light Source-Berkeley) have applied **COLTRIMS** recently, measuring the complete momentum balance in $(\gamma, 2e)$ reactions for different photon energies. They achieved a coincidence rate for the He-double ionization channel of about 100 coincidences per sec. In particular **COLTRIMS** will be a very powerful technique to study the angular distributions of the reaction products near the photo-ionization threshold. It can be applied to atomic as well to molecular targets.
Spielberger and coworkers [11, 23] have recently used **COLTRIMS** to measure the ratio of total cross sections of He double to single ionization by high-energy photon impact ($\hbar\omega = 9keV$ and $60keV$), respectively. **COLTRIMS** provides a clean method to separate the photo-effect and Compton-effect induced ionization processes. In case of photo-ionization the recoil-ion momentum is large and typically of the order of $\sqrt{2\hbar\omega}$ in $a.u.$. For a photon energy of $9keV$ the recoil momentum is approximately $25a.u.$. In case of Compton scattering the recoil ion is mostly a spectator and its final momentum is not very different from that in its initial state, and typically of the order of $1a.u.$. Using a "warm" super-sonic jet expansion [24] with a target density of about $2 \times 10^{12}\text{atoms}/cm^2$ the corresponding cross section ratios of single to double ionization of helium for photo-effect and Compton-effect was separately measured. Furthermore the Compton profile (*i.e.* the three-dimensional momentum distribution of the recoil ions for the Compton scattering process) was determined with very good statistics. In Figure 15a the density plot of the measured recoil-momentum distribution for He^{1+} ionization is presented. The outer ring distribution is due to photo-effect ionization and the inner spot is due to the Compton scattering process. Since in this experiment the photon beam had a broad energy distribution

(parasitic experiment using a "white light" beam at the HASYLAB) the photo-effect distribution must show a large momentum width too. In figure 15b and 15c the projection of the distribution on the direction of the electric field vector is shown for single (He^{1+}) and double ((He^{1+}) ionization.

5 Outlook and Perspectives

Because of its momentum resolution and high detection efficiency for slow recoil ions **COLTRIMS** is an excellent technique to study the momentum exchange in many-particle atomic collision processes. It is well suited to investigate the dynamics of inner-atomic many-electron processes by electron-recoil coincidence methods particularly for photo-ionization processes. Its application is, however, not restricted to the field of atomic collision physics. It may open new detection windows for other fields in physics, *e.g.* nuclear physics, where *e.g.* β-decay can be investigated with this method. The angular correlation between electron and neutrino and even the neutrino mass can be determined with improved precision. Using super-sonic gas jets or in the near future even laser cooled target devices, a recoil momentum resolution of 0.01 or even $0.001 a.u.$ may be feasible, if the recoil-ion trajectory and the recoil-ion TOF can be measured with the required precision. This requires large position-sensitive detection devices which can be developed from existing technology. The momentum of the emitted electron has to be measured as well (emission angle and TOF) with equivalent precision. These coincidence measurements provide detailed information on the electron-neutrino angular correlation. With sufficiently large detection devices (several meters diameter) a neutrino-momentum resolution of a few eV/c seems feasible. One notes that in such a measurement the neutrino mass can, in principle, be derived from one single decay event. Using laser cooled targets even polarized target nuclei can be provided.

Last but not least, using very cold molecular targets, the Coulomb explosion of interesting molecules can be investigated [17, 26] The momenta of all emitted fragments can be measured with high precision by using multi-hit detection devices, if all (except one) of these fragments are ionized. Also here a momentum resolution of $0.02 a.u.$ seems feasible.

6 Acknowledgement

This work was supported by DFG, BMBF(former BMFT), the Max-Planck-Forschungspreis of the Humboldt-Stiftung, Feodor-Lynen-Programm der Humboldt-Stiftung (R.D.) Graduierten Förderung des Landes Hessen (L.S.), Graduiertenkolleg-Schwerionenphysik (M.A.), Studienstiftung des Deutschen Volkes (V.M.), Willkomm-Stiftung, DAAD (I.A. and K.K.), and the Chemical Sciences Division, Office of Basic Energy Sciences, U.S. DOE. Furthermore we are indebted for many helpful discussions to our colleagues and friends R. Dreizler, H. J. Lüdde, J.Ast, S. Keller, R. E. Olson, M. Schulz, J. Burgdörfer, W. E. Meyerhof and U .Buck.

References

[1] O. Schwarzkopf, B. Krässig, J. Elmiger, and V. Schmidt. *Phys. Rev. Lett.*, 70:3008, 1993.

[2] O. Schwarzkopf, B. Krässig, V. Schmidt, F. Maulbetsch, and J. Briggs. *J. Phys.*, B27:L347–50, 1994.

[3] A. Huetz, P. Lablanquie, L. Andric, P. Selles, and J. Mazeau. *J. Phys.*, B27:L13, 1994.

[4] A. Lahmam-Bennani, C. Dupré, and A. Duguet. *Phys. Rev. Lett*, 63:1582, 1989.

[5] M.A. Coplan et al. *Rev.Mod.Phys.*, 66:985, 1994, and References therein.

[6] R. Dörner, V. Mergel, R. Ali, U. Buck, C.L. Cocke, K. Froschauer, O. Jagutzki, S. Lencinas, W.E. Meyerhof, S. Nüttgens, R.E. Olson, H. Schmidt-Böcking, L. Spielberger, K. Tökesi, J. Ullrich, M. Unverzagt, and W. Wu. *Phys. Rev. Lett*, 72:3166, 1994.

[7] W. Wu, R. Ali, C.L. Cocke, V. Frohne, J.P. Giese, B. Walch, K.L. Wong, R. Dörner, V. Mergel, H. Schmidt-Böcking, and W.E. Meyerhof. *Phys. Rev. Lett*, 72,:3170, 1994.

[8] R. Moshammer, J. Ullrich, M. Unverzagt, V. Schmidt, P. Jardin, R.E. Olson, R. Mann, R. Dörner, V. Mergel, U. Buck, and H. Schmidt-Böcking. *Phys. Rev. Lett*, 73:3371, 1994.

[9] V. Mergel, R. Dörner, J. Ullrich, O. Jagutzki, S. Lencinas, S. Nüttgens, L. Spielberger, M. Unverzagt, C.L. Cocke, R.E. Olson, M. Schulz, U. Buck, E. Zanger, W. Theisinger, M. Isser S. Geis, and H. Schmidt-Böcking. *Phys. Rev. Lett.*, 74, 1995.

[10] R. Dörner, T. Vogt, V. Mergel, H. Khemliche, S. Kravis, C.L. Cocke, J. Ullrich, M. Unverzagt, L. Spielberger, M. Damrau, O. Jagutzki, I. Ali, B. Weaver, K. Ullmann, C.C. Hsu, M. Jung, E.P. Kanter, B. Sonntag, M.H. Prior, E. Rotenberg, J. Denlinger, T. Warwick, S.T. Manson, and H. Schmidt-Böcking. *Phys. Rev. Lett.*, 1996. accepted for publication.

[11] L. Spielberger, O. Jagutzki, R. Dörner, J. Ullrich, U. Meyer, V. Mergel, M. Unverzagt, M. Damrau, T. Vogt, I. Ali, Kh. Khayyat, D. Bahr, H.G. Schmidt, R. Frahm, and H. Schmidt-Böcking. *Phys. Rev. Lett.*, 74:4615, 1995.

[12] R. Dörner, V. Mergel, L. Spielberger, O. Jagutzki, S. Nüttgens, M. Unverzagt, H. Schmidt-Böcking, J. Ullrich, R.E. Olson, K. Tökesi, W.E. Meyerhof, W. Wu, and C.L. Cocke. *AIP Conf. Proc. 360 (1995) Editors: L.J. Dube, J.B.A. Mitchell J.W. McConckey C.E. Brion*, AIP Press New York, 1995.

[13] G. Brusdeylins, J.P. Toennies, and R. Vollmer. page 98, Perugia, 1989.

[14] V. Mergel. *Phd thesis Universität Frankfurt*, 1996.

[15] T. Kambara, J.Z. Tang, Y. Awaya, B.D. dePaola, O. Jagutzki, Y. Kanai, M. Kimura, T.M. Kojima, V. Mergel, Y. Nakai, H.W. Schmidt-Böcking, and I. Shimamura. Three-dimensional recoil-ion momentum analyses in 8.7 mev o^{7+}-He collisions. *J. Phys.*, 1995. accepted for publication.

[16] M. Unverzagt et. al. *Phys. Rev. Lett.*, 76, 1996.

[17] R. Moshammer, M. Unverzagt, W. Schmitt, J. Ullrich, , and H. Schmidt-Böcking. *Rev. Sci. Instr.*, :submitted for publication, 1996.

[18] R. Dörner, J. Feagin, C.L. cocke, O. Jagutzki, M. Jung, E.P. Kanter, H. Khemliche, S. Kravis, V. Mergel, M.H. Prior, H. Schmidt-Böcking, L. Spielberger, J. Ullrich, M. Unverzagt, and T. Vogt. *Phys. Rev. Lett.*, 1996. submitted for publication.

[19] V. Mergel, R. Dörner, J. Ullrich, O. Jagutzki, S. Lencinas, S. Nüttgens, L. Spielberger, M. Unverzagt, C.L. Cocke, R.E. Olson, M. Schulz, U. Buck, and H. Schmidt-Böcking. *Nucl. Instr. Meth.*, 98, 1995.

[20] H.-P. Hülskötter, B. Feinberg, and W.E. Meyerhof. *Phys. Rev.*, A44:1712, 1991.

[21] E.C. Montenegro, W.S. Melo, W.E. Meyerhof, and A.G. dePinho. *Phys. Rev. Lett*, 69:3033, 1992.

[22] T. Vogt. *Diploma Thesis, University Frankfurt 1995, to be published.*

[23] L. Spielberger, O. Jagutzki, B. Krässig, U. Meyer, Kh. Khayyat, V. Mergel, Th. Tschentscher, Th. Buslaps, H. Bräuning, R. Dörner, T. Vogt, M. Achler, J. Ullrich, D.S. Gemmel, and H. Schmidt-Böcking. *Phys. Rev. Lett.*, submitted for publication.

[24] O. Jagutzki, L. Spielberger, R. Dörner, s: Nüttgens, V. Mergel, H. Schmidt-Böcking, J. Ullrich, R.E. Olson, and U. Buck. *Zeitschrift für Physik*, D36:5, 1996.

[25] S. E. Sobottka and M. B. Williams, *IEEE Trans Nucl. Sci.*, 35 348-351, 1988.

[26] I. Ali, R. Dörner, O. Jagutzki, J. Ullrich, K. Ullmann, and H. Schmidt-Böcking. in preparation.

[27] P. Jardin et al. to be submitted.

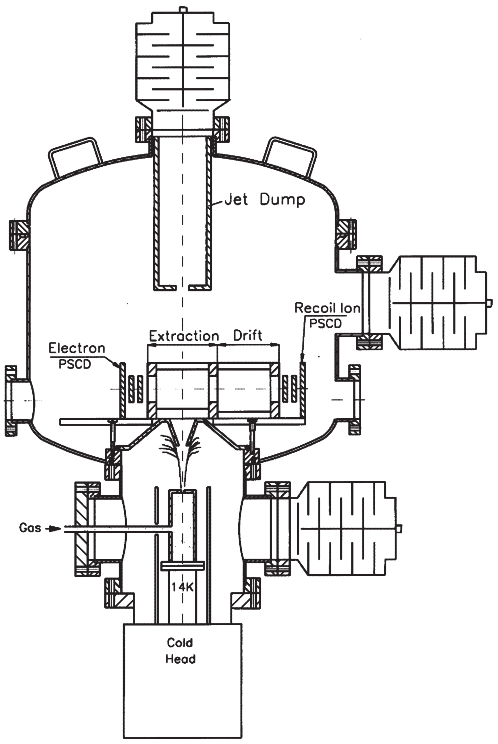

Figure 5: The upper part shows the target chamber with the recoil ion spectrometer: the lower part the source chamber where the gas jet is created by expanding through the $30\mu m$ nozzle, mounted on the cold head of a cryogenic system.

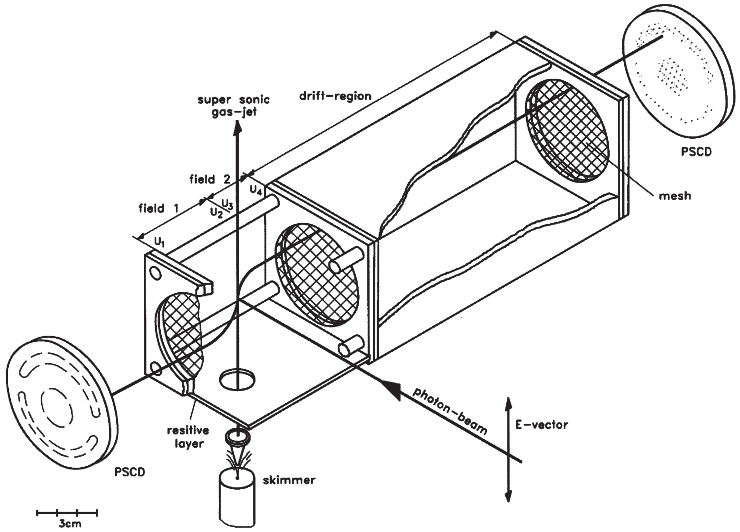

Figure 6: High-resolution recoil-ion momentum spectrometer with precooled supersonic gas jet target. ([10, 14])

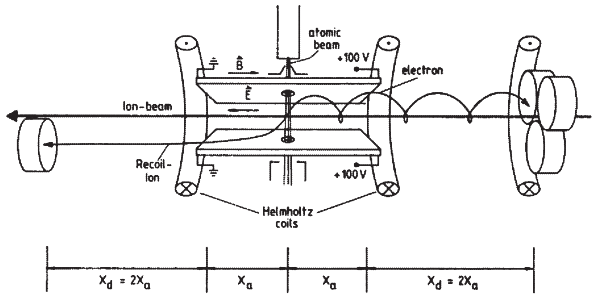

Figure 7: Recoil-ion spectrometer with solenoid field for collecting the electrons on a position-sensitive detector. The electric field is generated by carbon-coated ceramic plates parallel to the beam axis. [17]

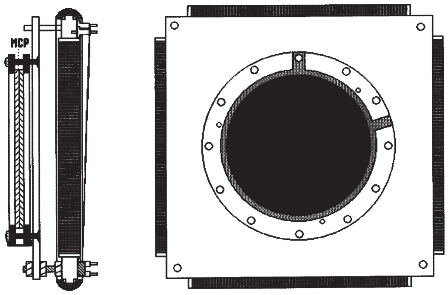

Figure 8: Scematic of a MCP detector with about 50mm active diameter and delay-line readout [25].

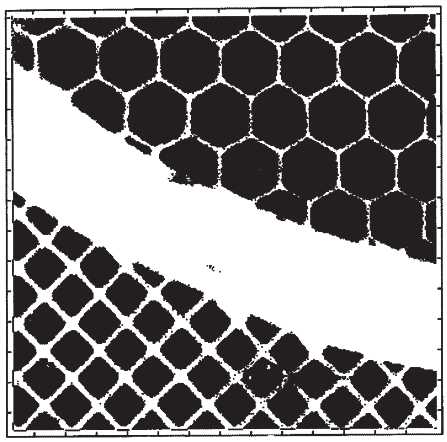

Figure 9: Shadow image of a wire mask. The MCP was homogeniously irradiated with an α-source. The picture shows an area of approximately $20mm \times 20mm$, the hexagonal wires have $0.2mm$ diameter. A Position resolution of better than $50\mu m$ can easily be obtained

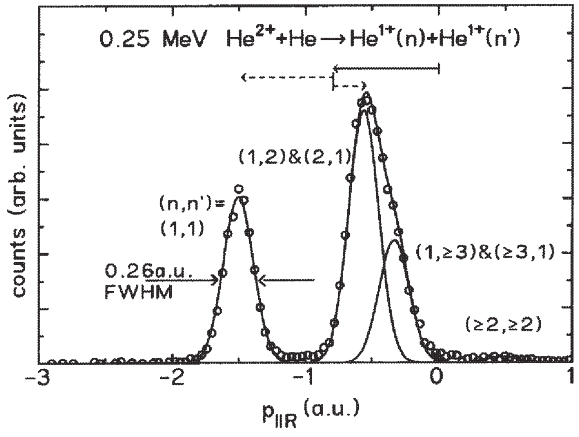

Figure 10: Longitudinal momentum distribution for the recoil ions from the reaction 0.25MeV and 1MeV He^{2+} + He $\rightarrow$ He^{1+} + He^{1+}. The momentum resolution is $0.26 a.u.$ FWHM. The peaks correspond to the different states of projectile and target as indicated in the figure. The full arrow shows the contribution of the term $qv_P/2$ from equation 1, which is due to the mass transfer between target and projectile; the dashed arrows show the Q/v_P-term from equation 1 for the different states. (From [9])

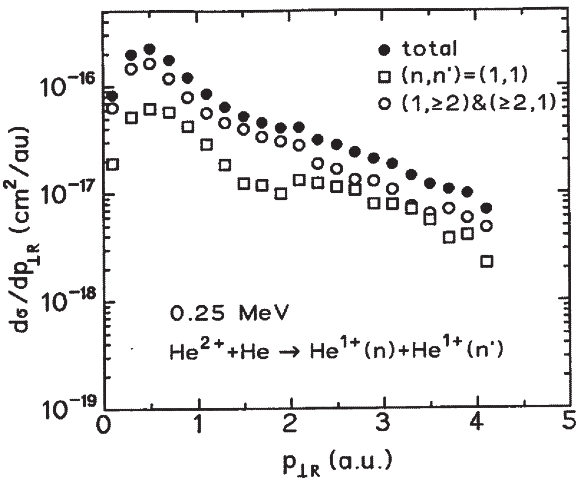

Figure 11: Differential state-selective capture cross sections. The x axis shows the transverse momentum of the recoil ion $p_{\perp R}$, which is equivalent to the projectile scattering angle ϑ_P ($\tan\vartheta_P = p_{\perp R}/p_0$, where p_0 is the incoming projectile momentum).
Full circles: sum over all states, squares: both partners are in ground state, open circles: one collision partner in some excited state. (From [9])

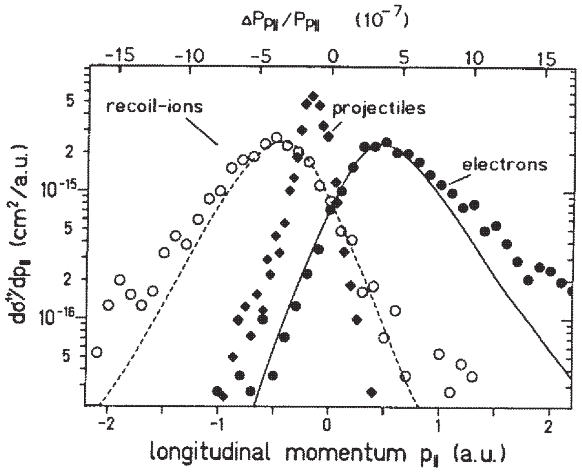

Figure 12: Longitudinal momentum distribution of electrons (full circles) and recoil ions (open circles) for single ionization of He by $3.6 MeV/u$ Ni^{24+} impact. The diamonds show the momentum change of the projectile. Full and dashed lines are results of nCTMC calculations.

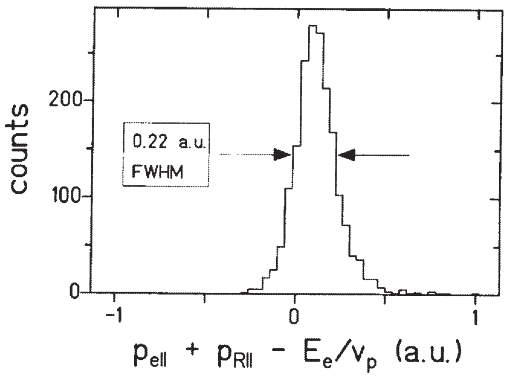

Figure 13: Projectile energy loss distribution as function of correlated longitudinal momenta of recoil ion and electron.

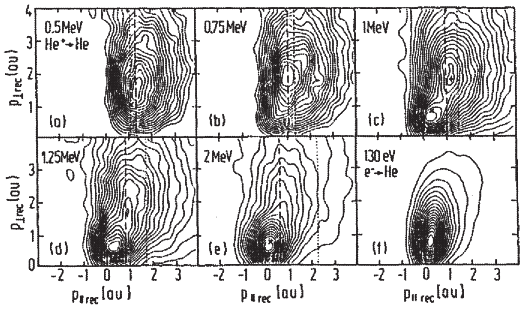

Figure 14: Doubly differential cross sections for reaction 3. The y axis shows the recoil transverse, the x axis the recoil longitudinal momentum. The contour lines represent a linear plot.

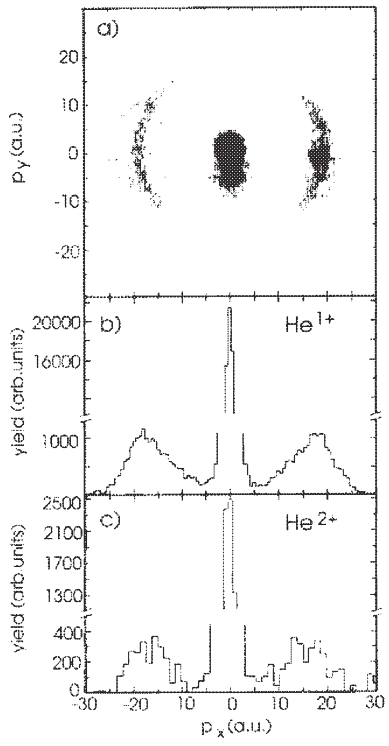

Figure 15: Measured He^{1+}-momentum distribution in the plane perpendicular to the photon-beam direction.